Iğdır Üniversitesi Fen Bilimleri Enstitüsü Dergisi, 15(3), 1019-1031, 2025
Journal of the Institute of Science and Technology, 15(3), 1019-1031, 2025

ISSN: 2146-0574, eISSN: 2536-4618

Kimya / *Chemistry* **DOI: 10.21597/jist.1647816**

Araştırma Makalesi / *Research Article*

Geliş tarihi / *Received*: 27.02.2025 **Kabul tarihi / *Accepted*: 10.04.2025**

Atıf İçin: Aygün Çağlar, M**. (**2025). Asidik ve Alkalin Elektrolitlerde Elektrokimyasal Hidrojen Üretimi için Sürdürülebilir bir Yöntemle $RuTe_2$ Dekore Edilmiş Karbon Nanofiberlerin Sentezi. *Iğdır Üniversitesi Fen Bilimleri Enstitüsü Dergisi*, 15(3), 1019-1031.

To Cite: Aygün Çağlar, M. (2025). $RuTe_2$ Decorated Carbon Nanofiber Electrocatalyst Synthesized via a Sustainable Method for Electrochemical Hydrogen Evolution in Acidic and Alkaline Electrolytes. *Journal of the Institute of Science and Technology*, 15(3), 1019-1031.

Asidik ve Alkalin Elektrolitlerde Elektrokimyasal Hidrojen Üretimi için Sürdürülebilir bir Yöntemle $RuTe_2$ Dekore Edilmiş Karbon Nanofiberlerin Sentezi

Mehtap AYGÜN ÇAĞLAR[1*]

Öne Çıkanlar:

- $RuTe_2$ dekore edilmiş GNF' basit, sürdürülebilir ve düşük maliyetli bir yöntemle sentezlendi
- $RuTe_2$ nanopartiküllerinin GNF içinde ve dış yüzeyinde homojen dağılımı gözlendi
- $RuTe_2$ dekore edilmiş GNF, hem alkalin hem de asidik ortamlarda Pt/C'ye göre etkili ve karşılaştırılabilir bir HER aktivitesi gösterdi

Anahtar Kelimeler:

- Rutenyum ditellürid
- Grafitize olmuş karbon nanofiber
- 1D Hibrit nanomalzemeler
- Hidrojen üretim reaksiyonu
- Elektrokataliz

ÖZET:

Rutenyum ditellürid ($RuTe_2$) katalizörü, grafitize olmuş karbon nanofiberler (GNF) üzerine dekore edilerek basit, çevre dostu ve düşük maliyetli özgün bir yöntem geliştirerek sentezlendi. Karakterizasyon çalışmaları, kristalin $RuTe_2$ nanopartikül oluşumların hem GNF destek malzemesinin iç kısmındaki kıvrımlı karbon kenarlarında, ortalama ~4 nm nanopartikül boyutu ile, hem de GNF'nin dış yüzeyinde homojen bir şekilde dağılım gösterdi. $RuTe_2$/@GNF'nin hidrojen evrim reaksiyonundaki elektrokimyasal performansı hem asidik hem de alkali ortamlarda araştırıldı. Sonuçlar, ticari aktif karbon üzerine dekore edilmiş platin nanopartiküllerinin (Pt/C), GNF ve metalik rutenyum nanopartiküllerinin GNF üzerine dekore edildiği malzemelerin HER sonuçlarıyla karşılaştırıldı. Sonuçlar, GNF destekli $RuTe_2$'nin son teknoloji Pt/C katalizörüne benzer bir HER performansı sergilediğini ve diğer kontrol materyallerinin HER aktivitesini bastırdığını gösterdi. Artan HER aktivitesi, HER için nano ölçekli bir ortamda kararlı ve aktif katalitik bölgelerin oluşmasını sağlayan GNF iç kısmındaki kıvrımlı kenarlarının sınırlı alanına atfedildi. Dahası, yüksek iletkenliğe sahip GNF destek malzemesi, nanopartiküller ile makroskobik elektrot arasında etkili bir elektrik köprüsü işlevi gördü. Bu yapılandırma, yalnızca elektrolit ile katalizör arasında verimli yük transferini kolaylaştırmakla kalmadı, aynı zamanda genel performansı da artırdı. Sonuç olarak, $RuTe_2$/@GNF her iki ortamda da çift işlevli bir katalizör görevi görerek gelişmiş proton adsorpsiyon/desorpsiyon sürecini kolaylaştırdı ve suyun elektrokimyasal ayrışma bariyerlerinin etkili bir şekilde aşılması sağlandı. Bu çalışma, geleneksel platin katalizörlerine alternatif olan yeni sürdürülebilir rutenyum kalkojenür bazlı katalizörlerin geliştirilmesinin önünü açmakta ve bunların verimli hidrojen üretimi için potansiyel kullanımlarını vurgulamaktadır.

$RuTe_2$ Decorated Carbon Nanofiber Electrocatalyst Synthesized via a Sustainable Method for Electrochemical Hydrogen Evolution in Acidic and Alkaline Electrolytes

Highlights:

- A novel two-step procedure was developed for the simple, sustainable, and low-cost sythesis of $RuTe_2$ decorated GNF
- $RuTe_2$ nanoparticles exhibited a homogeneous distribution inside and external of GNF
- $RuTe_2$ decorated GNF exhibited an effective and comparable HER activity to Pt/C both in alkaline and acidic mediums

Keywords:

- Ruthenium ditelluride
- Graphitized carbon nanofibers
- 1D Hybrid nanomaterials
- Hydrogen evolution reaction
- Electrocatalysis

ABSTRACT:

A novel ruthenium ditelluride ($RuTe_2$) catalyst supported by graphitized carbon nanofibers (GNF) has been synthesized developing a straightforward, environmentally friendly, and cost-effective method. Characterization studies indicated that the formation of crystalline $RuTe_2$ nanoparticles uniformly immobilized at the step edges within the internal cavity of GNF support, with an average nanoparticle size of ~4 nm, as well as the external surface of GNF. The electrocatalytic performance of $RuTe_2$/@GNF in the hydrogen evolution reaction was investigated in both acidic and alkaline mediums. The results were compared with those of commercial platinum nanoparticles on activated carbon (Pt/C), as well as with hollow GNF and GNF-supported metallic ruthenium nanoparticles. The results indicated that GNF-supported $RuTe_2$ exhibited a comparable HER performance to state-of-the-art Pt/C catalyst and suppressed the HER activity of other control materials. Increased HER activity was attributed to the confined space of step edges enabled the robust and active catalytic sites and facilitated the HER in a nanoscale environment. Additionally, the highly conductive GNF support functioned as an effective electrical bridge between the nanoparticles and the macroscopic electrode. This configuration not only facilitated efficient charge transfer between the electrolyte and the catalyst but also enhanced overall performance. As a result, $RuTe_2$/@GNF served as a bifunctional catalyst in both mediums, facilitating enhanced proton adsorption/desorption process and effectively overcoming water dissociation barriers. This study paves the way for developing novel sustainable ruthenium chalcogenide-based catalysts that are alternatives to traditional platinum catalysts, highlighting their potential use for efficient hydrogen generation.

[1] Mehtap AYGÜN ÇAĞLAR (**Orcid ID:** 0000-0003-2860-0908), Erzurum Technical University, Faculty of Science, Basic Sciences Department, Erzurum, Türkiye

***Sorumlu Yazar/*Corresponding Author**: Mehtap AYGÜN ÇAĞLAR, e-mail: mehtap.aygun@erzurum.edu.tr

INTRODUCTION

The decreasing fossil fuel supplies are leading to a global energy crisis, which in turn is prompting stronger efforts to discover alternative renewable energy sources and reduce the environmental damage caused by fossil fuels (Wei et al.,2019; Wu et al., 2023). Hydrogen is becoming increasingly recognized as a clean, storable, and transportable fuel, thanks to its higher energy density in comparison to traditional fossil fuels. Hydrogen can be produced using electrocatalysis of water, which is regarded as one of the most promising hydrogen generation technologies offering a sustainable and important alternative to fossil fuel-based energy sources in a zero-carbon-emission process. Hydrogen evolution reaction (HER), a half reaction of water electrolysis occurs at the cathode (Wei et al.,2019; Wu et al., 2023). It exhibits different reaction paths depending on the pH of the electrolyte (Yang et al., 2021). Compared to HER in acidic electrolytes, HER in alkaline electrolytes requires additional energy due to the slow water dissociation rates (Hu et al., 2019). Therefore, it is essential to develop efficient bifunctional catalytic systems not only enable fast proton adsorption process but also reducing the energy consumption related to water dissociation to accelerate the reaction kinetics. Platinum-based electrocatalysts stand out for their exceptional HER activity and kinetics, as they effectively overcome the thermodynamic potential barrier of 0 V at room temperature and under atmospheric pressure conditions (Wei et al., 2019; Lin et al., 2024). However, the high cost of Pt-based materials highlights the need for the development of more affordable and active electrocatalyst systems for HER. Sabatier principle states that the adsorption of reactants in catalytic reactions can inhibit weak binding reactions, while strong binding can coat the surface and limit the availability of sites for additional reactants (Medford et al., 2015; Hu et al., 2021)). It is suggested that optimal catalytic activity occurs when the interactions between reactants are of medium strength and positioned appropriately. Therefore, developing a HER catalyst alternative to Pt with optimal binding energies for both hydrogen and hydroxyl intermediates is also crucial to enhance HER activity in a variety of pH medium. Ruthenium exhibits a hydrogen binding energy comparable to that of platinum, while demonstrating superior corrosion resistance relative to platinum (Zhang et al., 2021). It is also available at almost one-fourth the cost of platinum (Yu vd., 2019; Hu et al, 2019). Moreover, ruthenium, which has a rich electron density compared to platinum, is also considered an alternative HER catalyst to platinum as it enables lower energy requirements for the water dissociation in the alkaline electrolyte (Zheng et al., 2016; Hu et al., 2019; Hu et al., 2022; He et al., 2022). Therefore, ruthenium-based electrocatalytic systems are considered promising HER catalysts to replace Pt-based catalyst.

Although ruthenium-based catalysts show significant potential in acidic and alkaline HER, their fundamental research and industrial applications are still in the early stages. Recently, Ru-based transition metal dichalcogenides (TMDCs) is great of interest as a promising alternative HER catalysts to Pt due to their earth abundance, low-cost and high activity in electrocatalytic hydrogen production (Gu et al., 2020; Zhang et al., 2021; Mondal et al., 2022; He et al., 2024; Li et al., 2024). Ruthenium chalcogenides are notable for their negative binding energies, which enable the easy capture of water molecules and -OH adsorption capabilities (Zhang et al., 2021; Lin et al., 2024)). Additionally, the tendency of nanoparticles to aggregate poses a considerable challenge that must be addressed to maintain the availability of catalytically active sites for HER applications. It is well-known that the HER activity of metal catalyst systems is enhanced using carbon-based support materials that enable the efficient dispersion and stabilization of metal catalyst, and provide good electrical conductivity in electrochemical

hydrogen production, (Luo et al., 2020; Gu et al., 2020; Yang et al., 2021; Aygün et al., 2021; Zhang et al., 2021; Li et al., 2023; He et al., 2024; Kuang et al., 2024; Lin et al., 2024). For example, Zhang et al. (2021) synthesized ruthenium dichalcogenides on multiwalled carbon nanotubes (CNT) by thermal annealing of pre-formed $RuCl_3$-deposited CNT materials at temperatures ranging from 700 to 1000 °C in the presence of sulfur, selenium, and tellurium chalcogen precursors. The resultant RuX_2/CNT materials (X: Se, S, Te) exhibited multiple crystal planes due to the variations in annealing temperature. Notably, the utilization of $RuTe_2$ in the marcasite phase demonstrated enhanced HER activity. He and his co-workers (2024) have recently investigated the electrochemical HER activity of ruthenium chalcogenides supported on carbon nanofibers (CNF) in both acidic and alkaline environments. The catalysts were prepared using a three-step method, starting with a $RuCl_3$ precursor and polyacrylonitrile (PAN) to synthesize $RuCl_3$@PAN nanofibers in dimethylformamide (DMF) solvent through electrospinning. Next, the material underwent an oxidation process at 270 °C, followed by carbonization at 800 °C, which converted it into metallic ruthenium-decorated carbon nanofibers. Finally, they thermally annealed the material at 700 °C to produce ruthenium-based chalcogenide nanoparticles supported on CNF. While these materials demonstrate high catalytic activity for hydrogen evolution reactions, the process of preparing carbon supported ruthenium chalcogenide-based nanoparticle catalysts is often complex. It involves extremely high temperatures for both the pretreatment of carbon support and/or the pyrolysis of Ru-based precursors, and it relies on solvents that are not environmentally friendly. Therefore, it is essential to explore solvent-free, straightforward, and cost-effective methods for their preparation in order to design highly active ruthenium chalcogenide-based HER catalysts.

In this study, a simple two-step solvent-free eco-friendly and low-cost procedure was developed to prepare highly active and crystalline ruthenium ditelluride nanoparticles ($RuTe_2$) immobilized within and external of the graphitized carbon nanofiber (GNF) for use as a catalyst in the electrochemical hydrogen evolution reaction. In this approach, GNF supported triruthenium dodecarbonyl ($Ru_3(CO)_{12}$) molecules was initially prepared in vapor phase and then $RuTe_2$/@GNF was synthesized by the thermal decomposition of the carbonyl groups and subsequent tellurization process through a chemical vapor deposition (CVD) setup. A combination of transmission electron microscopy (TEM), powder X-ray diffraction (XRD), energy dispersive X-Ray (EDX), and Raman spectroscopy was employed to characterize the morphological and structural properties of $RuTe_2$ nanoparticles on GNF. The electrocatalytic performance of $RuTe_2$/@GNF in hydrogen evolution reaction was then examined in both acidic and alkaline electrolytes, comparing the results with those of commercial platinum nanoparticles on active carbon (Pt/C), as well as hollow GNF and GNF supported metallic ruthenium nanoparticles. The findings revealed that GNF-supported $RuTe_2$ acts as a bifunctional catalyst in both acidic and alkaline electrolytes enabling enhanced proton adsorption and overcoming water dissociation barriers, which could be a promising catalyst alternative to commercial Pt/C.

MATERIALS AND METHODS

Telluride powder, $Ru_3(CO)_{12}$ and Pt/C (%20 by weight) commercial catalyst were purchased from Sigma-Aldrich. Graphitised nanofibers were supplied by Pyrograf® Products Inc, USA. TEM analysis was performed using a Hitachi HighTech HT7700 microscope with an information limit of 0.144 nm at 120 kV at Atatürk University in Turkey. Samples for TEM analysis were prepared by dispersing the materials in HPLC grade iso-propanol under ultra-sonication, then depositing onto a lacey carbon film coated copper grid (Ted Pella, INC). An energy dispersive X-Ray spectroscopy (EDX) combined with a scanning electron microscope (SEM, Zeiss Sigma 300) was used for elemental analysis at atatürk

University. A Micro-Raman spectrometer (WITec alpha 300 R) at Atatürk University was used operating at a wavelength of 532 nm and a power of 0.3 mWatt. The powder X-ray diffraction patterns were obtained an XRD-GNR-Explorer X-Ray diffractometer equipped with a Cu-Ka radiation source (λ=1.54059 Å) operating at 40 kV and 30 mA, between 20° and 80°) at Erzurum Technical University in Turkey. Obtained data was compared with the International Diffraction Data Center (ICDD) standard data cards.

Catalyst Preparation

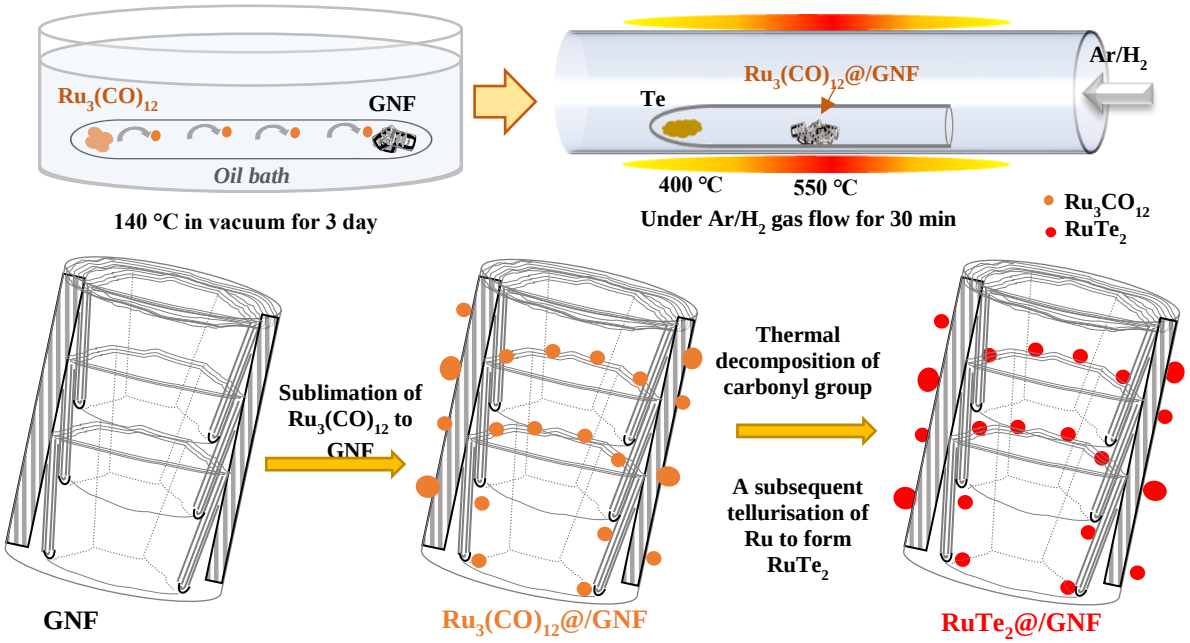

Figure 1. Schematic of the synthesis routes for $RuTe_2$/@GNF

Preparation of $RuTe_2$-encased GNF electrocatalyst: The length of GNF was reduced using via ball-milling process prior to use as a support (Aygun vd., 2021). $Ru_3(CO)_{12}$ deposited GNF was synthesized by combining a $Ru_3(CO)_{12}$ precursor (8,44 mg, masses equivalent to the %20 of Ru metal required in the final material) with a 20 mg of freshly shortened GNF (Aygün et al., 2021) in a Pyrex tube, and sealed under vacuum (10^{-5} bar). The tube was heated at 140 °C for 3 days in an oil bath and cooled in an ice bath. The hybrid material GNF was then removed from the tube. $RuTe_2$ encased GNF was synthesized by the thermal tellurization of $Ru_3(CO)_{12}$ encased GNF using a CVD setup. 10 mg of material and 25 mg powder of telluride were placed in the middle and edge of a one-end open quartz tube (1 cm in diameter), respectively. The tube was then located in the center of a CVD tube (1 inch in diameter and 80 cm in length), positioned in a horizontal furnace. The CVD tube was initially flushed with a 100 sccm of Ar gas, and heated to 120°C for 10 min to eliminate the any residual water in the tube. Ar gas flow was then set to 40 sccm and then a 10 scmm of H_2 gas was instantly introduced into the tube. The centre of the furnace was heated up to 550°C, where the position of Te powder was corresponding to a temperature of ~400 °C. The reaction was maintained at this temperature for 30 minutes and heating was stopped. The CVD tube was cooled down to the room temperature under gas flow and as grown material was then collected.

Preparation of Ru-encased GNF; A similar synthesis condition reported by Aygun et al., (2017) was followed.10 mg of $Ru_3(CO)_{12}$/@GNF powder was initially placed in a quartz crucible and located

in the middle of CVD tube. After flushing the tube by Ar flow at 120 C for 10 min, the furnace was set up to 550 C and maintained for 60 min under Ar flow. Material was then collected after cooling the tube to room temperature under Ar flow.

Electrochemical measurements

The electrochemical tests were conducted by a three-electrode setup using Autolab potentiostat PGSTAT204 with a glassy carbon electrode (GCE) (3 mm in diameter, Redox Instruments) as the working electrode, a graphite rod (Redox instruments) as a counter electrode and a reversible hydrogen electrode (RHE, HydroFlex) as the reference electrode, respectively. Autolab potentiostat was coupled with a NOVA software.

Preparation of working electrode: A catalyst ink solution was prepared for each catalyst where catalyst (1 mg) was dispersed in water (0.5 mL) under the ultrasonication for 15 mins, respectively. Each catalyst ink corresponding of a resultant metal loading of 85µg/cm$^2_{geo}$ were deposited onto the GCE with a 0.171 cm^2 geometric surface area by drop casting and then dried in air at room temperature. Commercial Pt/C and control catalyst electrodes were also prepared by the same procedure.

HER measurements were taken between 0.2 V and -0.9 V versus RHE at a sweep rate of 10 mV/s in nitrogen saturated 0.1M HClO4 and 0.1M KOH by the preparation of a fresh electrode each time from each catalyst at room temperature, respectively. Cyclic voltammetry (CV) measurements were taken between 0 and 1 V versus RHE before and after HER measurements. Impedance spectroscopy was used to measure the cell resistance (R) immediately before each HER measurements taking the AC impedance spectra from 32 to 0.1 kHz with a voltage perturbation of 10 mV. To calculate the cell resistance-free potential of the working electrode, the real part of the cell resistance was taken at 1 kHz and all of the I-E (current-potential) curves was corrected using the formulation of $E = E_{experimental}-(I*R)$.

RESULTS AND DISCUSSION

Graphitized carbon nanofiber (GNF) supported ruthenium ditelluride ($RuTe_2$) nanoparticles were prepared following a two stepwise synthesis procedure in which GNF was shortened prior to the use to eliminate the lenght depended mass transportation resistance in HER (Aygün et al. 2021) (Figure 1). Triruthenium dodecarbonyl ($Ru_3(CO)_{12}$) was selected as the precursor because of its lower sublimation temperature and the presence of labile carbonyl ligands. $Ru_3(CO)_{12}$ precursor was then combined with shortened GNF in a Pyrex tube and the tube was sealed under vacuum using a procedure reported in the literature (Aygün et al., 2017). In this approach, $Ru_3(CO)_{12}$ molecules in vapor phase were aimed to insert internal cavity of the nanofibers (@GNF) (Figure 1a). In the second step of the synthesis, a method was developed to form GNF supported $RuTe_2$ from $Ru_3(CO)_{12}$ deposited GNF using a chemical vapor deposition (CVD) setup. The resultant $Ru_3(CO)_{12}$/@GNF material was then moved to a one-end closed quartz tube in the presence of tellurium powder and located to the CVD tube. $RuTe_2$ nanoparticles was synthesized by the decomposition of carbonyl group and in-situ thermal tellurization process under a gas flow of hydrogen and argon mixture to ensure that the optimum tellurium transfer to the material by H_2Te. Transmission electron microscopy (TEM) imaging confirmed that the presence of nanoparticles in the form of spherical-like shape which were located both within GNF (@GNF) and adsorbed on the exterior of GNF (/GNF) (Figure 2b).

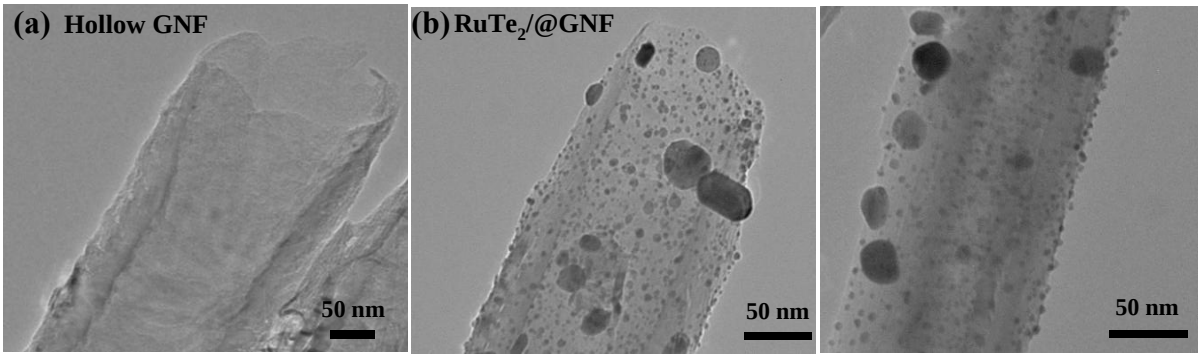

Figure 2. TEM images of (a) hollow shortened GNF and (b) $RuTe_2$/@GNF material.

Energy dispersive X-ray spectroscopy (EDX) coupled with a scanning electron microscope (SEM) confirmed the presence of Ru and Te in an atomic ratio of 1:1.93, which proved the formation of $RuTe_2$ (Figure 3a).

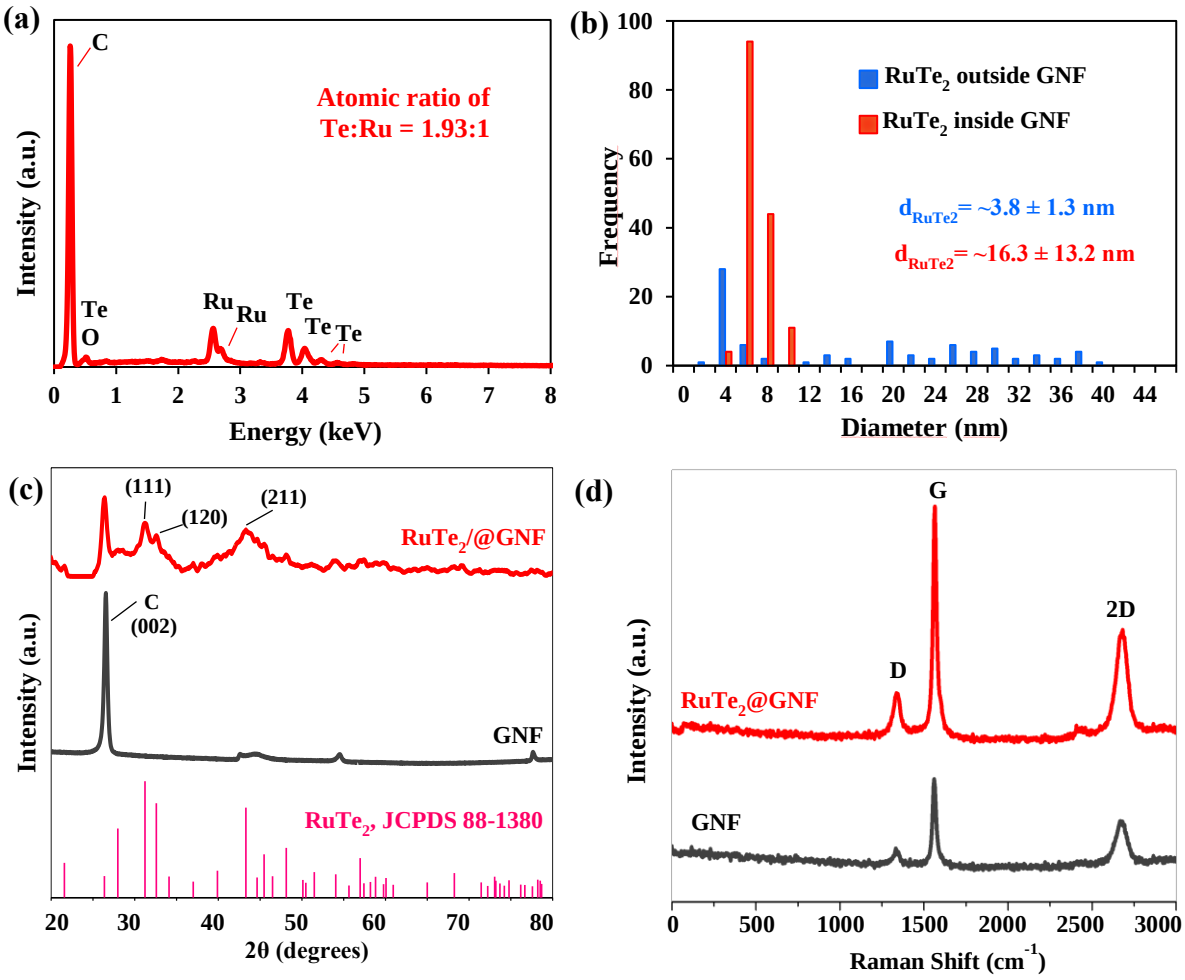

Figure 3. (a) EDX spectra of $RuTe_2$/@GNF. (b) Size distribution histogram of $RuTe_2$ nanoparticles in the $RuTe_2$/@GNF sample obtained by measuring the diameters of more than 100 spherical nanoparticles located internally of GNF (blue) and outside of GNF (red) for each via TEM images, respectively (c) XRD spectra of $RuTe_2$/@GNF using GNF as control, and JCPDS 88-1380 as reference XRD data of $RuTe_2$, respectively. (f) Raman spectra of $RuTe_2$/@GNF with GNF control

Size distribution studies conducted using TEM images of $RuTe_2$/@GNF focused on the nanoparticles located at the step edges within the GNF, as well as those external surface to it (Figure 3b). The analysis revealed that the $RuTe_2$ nanoparticles were uniformly dispersed and small in size,

measuring with a mean dimeter of approximately 3.8 ± 1.3 nm within the GNF. In contrast, the external surface of GNF displayed even smaller nanoparticles, with sizes less than 5 nm in mean diameter while a small fraction of $RuTe_2$ nanoparticles on the exterior of the GNF were relatively larger, accounting for less than 10% of the total nanoparticle count. Average nanoparticle size on external surface of GNF was about 16.3 ± 13.2 nm. This could be due to these larger particles could not benefitted from the same templating effect during the sublimation process of $Ru_3(CO)_{12}$ precursor and therefore become less uniform and larger in size. Powder XRD spectroscopy was used to identify the crystal structure of $RuTe_2$/@GNF using GNF as background, which exhibited the characteristic peak of GNF at ~26.57° corresponding to (002) plane of carbon, and two broad main peaks of $RuTe_2$ at ~31.21° and ~43.36°, corresponding to the (111) and (211) planes of a marcasite-type orthorhombic $RuTe_2$ (JCPDS, no:88-1380), respectively (Figures 3c). Raman spectra of $RuTe_2$/@GNF and GNF as control showed characteristic peaks of carbon nanofiber in the region of 1337.12 cm^{-1} (Defect or D band) and 1566.49 cm-1 (2D band) (Figure 3d) (Paleo et al., 2023). However, $RuTe_2$/@GNF indicated a lower intensity ratio between D and G bands as 0.48, compared to that of GNF as 0.68. This could be due to the interaction between $RuTe_2$ and GNF as a result of the electron transfer between each other altering the electronic properties of the material. Moreover, the defected GNF outermost surface due to the shortening process via ball-milling could be re-graphitized through the CVD process resulting the decrease in the defect band.

The electrocatalytic hydrogen evolution performance of $RuTe_2$/@GNF was examined using an electrochemical lineer sweep voltammetry (LSV) in hydrogen saturated aqueous 0.1M HClO4 and 0.1M KOH, respectively. The LSV polarization curves were obtained by the plots of current density normalized by dividing to the geometric surface area of the GCE versus the potential corrected by the ohmic resistant due to the interphase between the catalyst electrode and electrolyte solutions (Figure 4a and Figure 4b). HER activity of $RuTe_2$/@GNF was evaluated by the common parameters used in HER activity, i.e. onset HER potential, overpotential (η_{10}) value to achieve a current density of -10 mV/cm^2_{geo} and Tafel slopes for the determination of the acidic and alkaline HER mechanisms in the literature, respectively (Figure 4a and Table 1) (Wei et al., 2019). These parameters were also given for commercial Pt/C, as well as hollow GNF and Ru/@GNF controls to compare with that of $RuTe_2$/@GNF, respectively. Overpotential (η) values were obtained by the difference of potential applied and equilibrium potential versus RHE. After the all HER measurements, all these parameters were given in Table 1 for each material, including η_{20} values. As expected, commercial Pt/C showed the best HER activity in the agreement with the literature (Cheng et al., 2017; Luo et al., 2019; He et al., 2024). Pt/C exhibited an onset potential of 0 mV corresponding to the theoretical HER onset in both acidic and alkaline electrolytes (Figure 4a). $RuTe_2$/@GNF exhibited the Pt-like very small onset HER potentials with about -11 mV and -7 mV versus RHE in acidic and alkaline electrolytes, respectively.

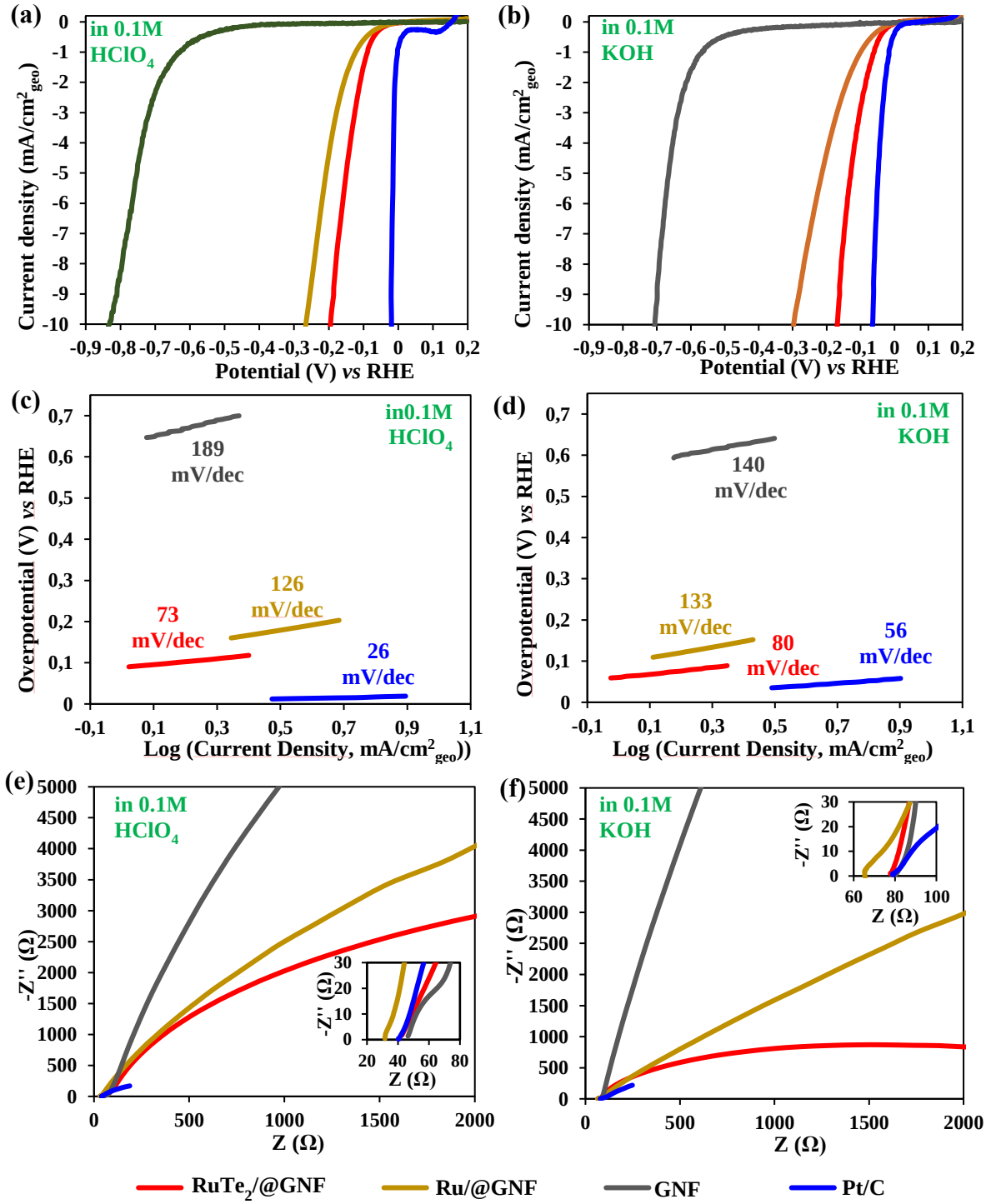

Figure 4. Electrochemical HER polarisation curves for $RuTe_2$/@GNF electrocatalyst in (a) acidic and (b) alkaline electrolytes. Tafel polots of $RuTe_2$/@GNF electrocatalyst in (c) acidic and (d) alkaline electrolytes. Impedance measurements for $RuTe_2$/@GNF electrocatalyst in (e) acidic and (f) alkaline electrolytes by potential cycling. Hollow GNF, Ru/@GNF and commercial Pt/C were used as controls in all measurements

Under both acidic and alkaline conditions, HER is driven by a two-electron transfer reaction in the presence of a catalyst following either Volmer-Heyrovsky of a Volmer-Tafel mechanisms (Bard and Faulkner, 2000; Wei et al., 2019; Wu et al., 2023). In an acidic electrolyte, protons (H^+) from the electrolyte are electrochemically adsorbed onto an active site on the catalyst (*), gaining an electron to

form a hydrogen intermediate during the Volmer step (Equation 1). After the Volmer step, adsorbed hydrogen intermediate can react either with another proton by gaining another electron (Equation 2) or with another adsorbed proton to form hydrogen gas (H_2) (Equation 3).

$$Volmer\ step: H^+ + e^- + * \rightarrow H^* \quad (1)$$

$$Heyrovsky\ step: H^* + H^+ + e^- \rightarrow H_2 + * \quad (2)$$

$$Tafel\ step: 2H^* \rightarrow H_2 + 2^* \quad (3)$$

In alkaline electrolytes, HER involves binding a water molecule to a metal catalyst, which is then split into a proton through the Volmer step (Equation 4). The reaction then follows either the Heyrowsky step (Equation 5) or the Tafel step (Equation 6).

$$Volmer\ step: H_2O + e^- + * \rightarrow H^* + OH^- \quad (4)$$

$$Heyrovsky\ step: H^* + H_2O + e^- \rightarrow H_2 + OH^- + * \quad (5)$$

$$Tafel\ step: 2H^* \rightarrow H_2 + 2^* \quad (6)$$

To discern the rate-determining step (RDE) in both acidic and alkaline HER, Tafel slopes were calculated by the simplified Butler-Volmer equation obtained from the slope b by the linear fitting between the overpotential to logarithmic current density (Equation 7).

$$\eta = a + b \log(j) \quad (7)$$

To determine the RDE for HER performance of platinum at room temperature, Tafel slopes values of 120, 40, or 30 mV/dec are considered for the Volmer, Heyrovsky, and Tafel steps, respectively (Yang et al., 2021). Pt/C demonstrated the faster Volmer-Tafel steps with a Tafel slope of 26 mV/dec in acidic electrolyte (Figure 4c). However, Pt/C indicated a relatively lower HER activity in alkaline electrolyte due to the slower HER kinetics, which followed the Volmer-Heyrowsky steps with a Tafel slope of 56 mV/dec (Figure 4d). On the contrary of Pt/C, $RuTe_2$/@GNF exhibited an improved HER activity in alkaline electrolyte compared to the HER in acidic electrolyte (Figure 4c-d). Moreover, hollow GNF also exhibited a better HER performance in alkaline similar to $RuTe_2$/@GNF, which proves the contribution of support in the enhanced HER activity. In contrast, the metallic Ru/@GNF control showed a better HER performance in acidic electrolytes.

Table 1. Summary of the onset potentials, overpotential at -10 and -20 mA/cm^2, and Tafel slopes obtained via LSV polarisation curve of $RuTe_2$/@GNF compared to those of Pt/C, Ru/@GNF and GNF

Catalyst	Onset Potential (mV)	η_{10} (mV)	η_{20} (mV)	Tafel Slopes (mVdec)	Electrolyte (0.1 M)
$RuTe_2$/@GNF	-11	190	258	73	$HClO_4$
	-7	169	218	80	KOH
Ru/@GNF	-21	266	377	126	$HClO_4$
	-27	297	453	133	KOH
GNF	-618	827	-	189	$HClO_4$
	-551	705	787	140	KOH
Pt/C	-0	20	32	26	$HClO_4$
	-0	64	108	56	KOH

*Overpotential (mV) at 10 mA/cm$^2_{geo}$ and 10 mA/cm$^2_{geo}$ was sembolized with η_{10} and η_{10} ,respectively

Moreover, $RuTe_2$/@GNF required an overpotential (η10) of 190 mV to achieve a current density of 10 mA/cm² in acidic conditions, compared to 169 mV in alkaline conditions. Although the Pt/C catalyst exhibited significantly lower η10 values of just 20 mV in acidic and 64 mV in alkaline

electrolytes, $RuTe_2$/@GNF showed notably lower η_{10} values compared to both Ru/@GNF and GNF controls in each electrolyte (Table 1). Impedance measurements further indicated the higher HER activity of $RuTe_2$/@GNF compared to those of the Ru/@GNF and GNF controls was accompanied with the its lower charge transfer resistance (Figure 4e-f). He et al. (2024) investigated the HER activity of carbon nanofiber supported ruthenium dichalcogenides including tellurium, sulfur and selenium and both in 0.5M H_2SO_4 and 1 M KOH. They observed an increased alkaline hydrogen evolution reaction activity when $RuTe_2$ was present, with an average particle size of about 20 nm. On the other hand, Zhang and coworkes (2021) studied the HER activity of CNT supported ruthenium dichalcogenides both in more concentric acidic and basic electrolytes, i.e. 0.5 M H_2SO_4 and 1 M KOH, and reported the superior acidic HER activity in the presence of marcasite-type $RuTe_2$, with an average particle size of about 7.1 nm. Furthermore, the enhanced HER performance of the bare GNF support indicates that it plays a crucial role in the overall activity of $RuTe_2$/@GNF. This is primarily due to the strong interactions between the $RuTe_2$ nanoparticles and the GNF supports. Moreover, the step edges within the internal cavity of the GNF help the formation and stabilization of smaller nanoparticles, leading to a greater number of accessible and active catalytic sites in a nanoscale confined environment for HER (Aygun et al., 2021). Additionally, the one-dimensional axial structure of the GNF and strong interactions with stabilized $RuTe_2$ nanoparticles facilitates an efficient electron transfer. On the other hand, superior HER performance of $RuTe_2$/@GNF compared to the metallic Ru/@GNF control proves that the presence of Te chalcogenides covalently interacted with Ru enhance the active sites of the catalyst compared to metallic Ru supported by GNF. All these factors play an important role on the higher HER activity over $RuTe_2$/@GNF.

The cyclic voltammetry (CV) profiles of $RuTe_2$/@GNF, GNF, and Pt/C were also investigated before and after HER measurements in both acidic and alkaline electrolytes, respectively (Figure 5). All catalysts exhibited a gradual decrease in both desorption/adsorption and oxidation/reduction peak areas after the HER measurements were conducted in an acidic electrolyte. Notably, both $RuTe_2$/@GNF and GNF support maintained stable CV characteristics, showing no change before and after HER measurements. In contrast, the commercial Pt/C catalyst demonstrated a marked decline in both peak areas, indicating a loss in activity. These results revealed that GNF supported $RuTe_2$ acts as a bifunctional catalyst in both acidic and alkaline environments. It enables more active sites available for proton adsorption and desorption, while also accelerating the dissociation of water molecules.

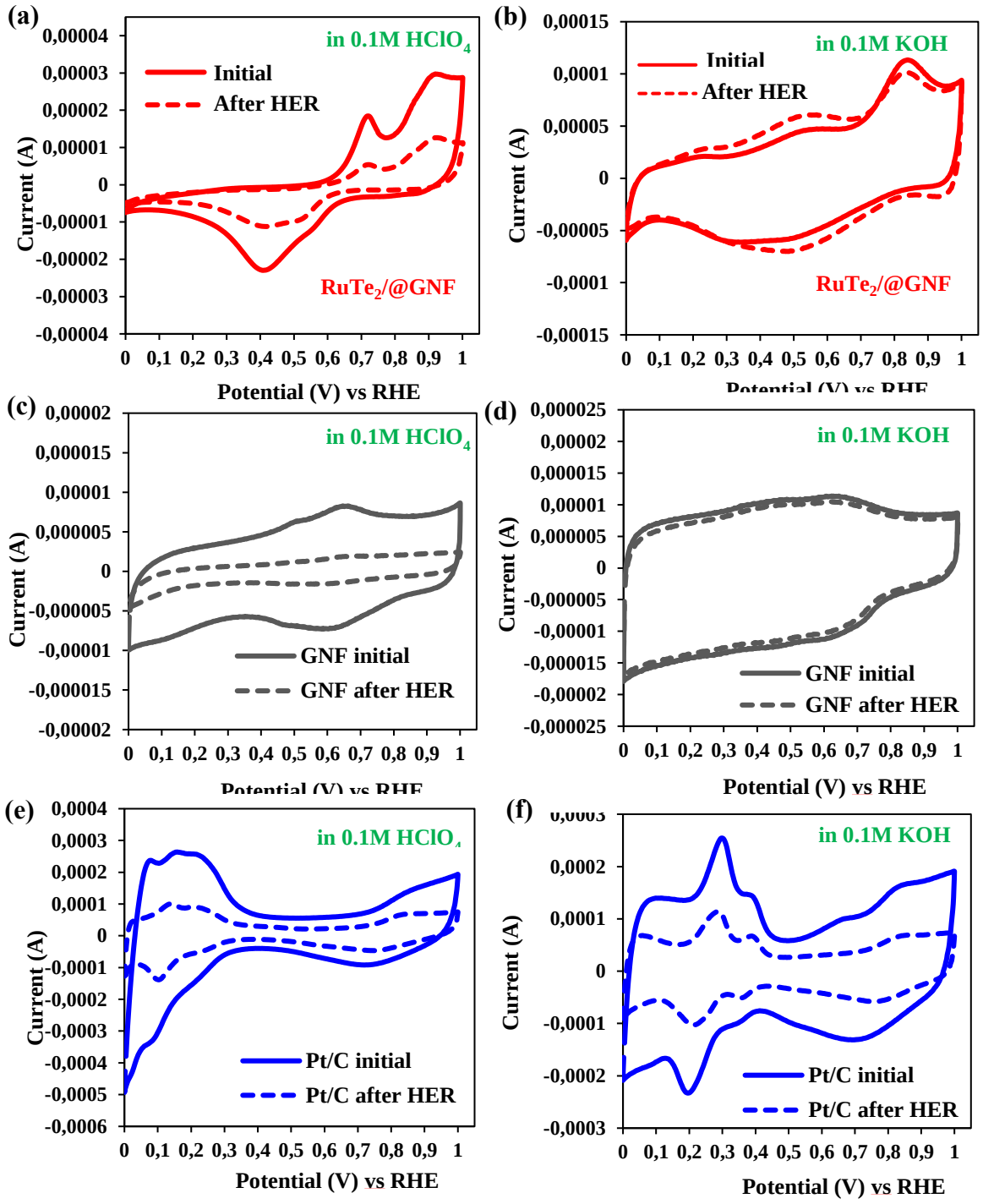

Figure 5. CVs of (a-b) $RuTe_2$/@GNF, (b-c) GNF support and (e-f) Pt/C in acidic and alkaline electrolytes before and after HER measurements

CONCLUSION

In summary, a novel GNF-supported $RuTe_2$ nanoparticle catalyst was successfully synthesized using a simple, eco-friendly and low-cost approach. Spectroscopy analyses coupled with imaging techniques revealed that $RuTe_2$ nanoparticles uniformly dispersed both within the interior channels and external surface of GNF. It exhibited impressive electrochemical hydrogen evolution performance comparable to that of platinum-based catalysts in both acidic and alkaline media. The effective hydrogen production capability of $RuTe_2$/@GNF was attributed to the strong interactions between the $RuTe_2$

nanoparticles and the highly conductive GNF carbon support. This arrangement not only enhances the availability of active sites but also facilitates efficient charge transfer between the catalyst and the electrolyte. These nanoparticles, particularly confined at the step edges within the GNF significantly increased the number of electrocatalytic active sites for HER and the local concentration of reaction intermediated. GNF support served dual functions: as nanoscale containers that anchor and protect catalytically active $RuTe_2$ nanoparticles, and as nanoelectrodes that provide an effective electric bridge between the nanoparticles and the macroscopic electrode. This configuration not only promoted effective charge transfer between the electrolyte and the catalyst but also markedly improved overall performance. As a result, GNF-supported $RuTe_2$ acted as a bifunctional catalyst enabling fast proton adsorption/desorption and water dissociation process. Overall, $RuTe_2$/@GNF catalyst, along with the simple, sustainable, and inexpensive synthesis technique and highly conductive GNF support, provided a promising alternative to costly and resource-dependent platinum-based catalysts. These results underscore the potential of $RuTe_2$/@GNF for large-scale, sustainable hydrogen generation and open avenues for creating more affordable, eco-friendly energy solutions. Future research should concentrate on the development of ruthenium-based transition metal chalcogenide-GNF carbon hybrid catalytic systems and evaluation the catalyst's performance, stability and scalability to satisfy the increasing demand for renewable energy source of hydrogen.

Conflict of Interest

The article author declares that there is no conflict of interest.

Author's Contributions

Mehtap Aygün Çağlar: study conception and design, investigation, data collection, analysis and interpretation of results, and manuscript preparation.

REFERENCES

Aygün, M., Stoppiello, C. T., Lebedeva, M. A., Smith, E. F., Gimenez-Lopez, M. del C., Khlobystov, A. N., Chamberlain, T. W. (2017). Comparison of alkene hydrogenation in carbon nanoreactors of different diameters: probing the effects of nanoscale confinement on ruthenium nanoparticle catalysis. *Journal of Material Chemistry A*, 5(40), 21467–21477.

Aygün, M., Guillen-Soler, M., Vila-Fungueiriño, J. M., Kurtoglu, A., Chamberlain, T., Khlobystov, A., Gimenez Lopez, M. del C. (2021). Palladium Nanoparticles Hardwired in Carbon Nanoreactors Enable Continually Increasing Electrocatalytic Activity During the Hydrogen Evolution Reaction. *ChemSusChem.* 14 (22), 4846-5074.

Bard, A. J. and Faulkner, L. R. (2000). Electrochemical Methods: Fundamentals and Applications, Jonh Wiley, New York.

Cheng, Y., Lu, S., Liao, F., Liu, L., Li, Y., Shao, M. (2017) Rh-MoS2 Nanocomposite Catalysts with Pt-Like Activity for Hydrogen Evolution Reaction. *Advance Functional Materials*. 27, 1700359, 1–6.

Gu, X., Yang, X., Feng, L. (2020). An Efficient RuTe2/Graphene Catalyst for Electrochemical Hydrogen Evolution Reaction in Acid Electrolyte. *Chemistry – An Asian Journal*. 15, 2886-2891.

He, Q., Zhou, Y., Shou, H., Wang, X., Zhang, P., Xu, W., Qiao, S., Wu, C., Liu, H., Liu, D., Chen, S., Long, R., Qi, Z., Wu, X., Song, L. (2022). Synergic reaction kinetics over adjacent ruthenium sites for superb hydrogen generation in alkaline media. *Advance Materials*,34, 2110604.

He, C., Wei, Y., Xu, J., Wei, Y., Wang, T., Liu, R., Ji, L., Liu, Z., Wang, S. (2024). Chalcogen-dependent catalytic properties of RuX_2 (X = S/Se/Te) nanoparticles decorated carbon nanofibers for hydrogen evolution in acidic and alkaline media. *Nano Research*, 17, 2528–2537.

Hu, C., Zhang, L., Gong, J., 2019. Recent Progress of Mechanism Comprehension and Design of Electrocatalysts for Alkaline Water Splitting, *Energy Environmental Science*,12, 2620-2645.

Hu, S.L.; Li, W.X. (2021). Sabatier principle of metal-support interaction for design of ultrastable metal nano-catalysts. *Science, 374*,1360–1365.

Hu, Q., Gao, K., Wang, X., Zheng, H., Cao, J., Mi, L., Huo, Q., Yang, H., Liu, J., He, C. (2022). Subnanometric Ru clusters with upshifted D band center improve performance for alkaline hydrogen evolution reaction. *Nature Communications*, *13*,3958.

Kuang, Y.B.; Yang, F.L.; Feng, L.G. Advancements in ruthenium (Ru)-based heterostructure catalysts: Overcoming bottlenecks in catalysis for hydrogen evolution reaction. *Adv. Energy Mater*. **2024**, *14*, 2402043.

Li, L., Tian, F., Qiu, L., Wu, F., Yang, W., Yu, Y. (2023) Recent progress on ruthenium-based electrocatalysts towards the hydrogen evolution reaction. *Catalysts*, *13*, 1497.

Li, J., Miró, R., Wrzesi´nska-Lashkova, A., Yu, J., Arbiol, J., Vaynzof, Y., Shavel, A., Lesnyak, V. (2024). Aqueous room-temperature synthesis of transition metal dichalcogenide nanoparticles: A sustainable route to efficient hydrogen evolution. *Advance Functional Materials*, 2404565

Lin, B.-L, Chen, X., Niu, B.-T., Lin, Y.-T., Chen, Y.-X., Lin, X.-M. (2024). The Research Progress of Ruthenium-Based Catalysts for the Alkaline Hydrogen Evolution Reaction in Water Electrolysis. *Catalysts, 14*, 671.

Luo W, Gan J, Huang Z, Chen W, Qian G, Zhou X, Duan X. (2019). HER performance of Pt-based catalysts immobilized on functionalized vulcan carbon by atomic layer deposition. *Frontier Materials*, 6:251.

Luo, W.J., Wang, Y.J., Cheng, C.W. (2020). Ru-based electrocatalysts for hydrogen evolution reaction: Recent research advances and perspectives. *Material Today Physic*, *15*, 100274.

Medford, A. J., Vojvodic, A., Hummelshøj, J. S., Voss, J., Abild-Pedersen, F., Studt, F., Bligaard, T., Nilsson A., Nørskov, J. K., 2015. From the Sabatier principle to a predictive theory of transition-metal heterogeneous catalysis, Catalysis, 328, 36–42.

Mondal, A., Vomiero, A. (2022). 2D transition metal dichalcogenides-based electrocatalysts for hydrogen evolution reaction. *Advance Functional Materials, 32*, 2208994.

Paleo, A.J., Krause, B., Mendes, A.R., Tavares, C.J., Cerqueira, M.F., Muñoz, E., Pötschke, P. (2023). Comparative Thermoelectric Properties of Polypropylene Composites Melt-Processed Using Pyrograf® III Carbon Nanofibers. *Journal of Composites Science.*7, 173.

Yang, Y., Yu, Y., Li, J., Chen, Q., Du, Y., Rao, P., Li, R., Jia, C., Kang, Z., Deng, P., Shen, Y., Tian, X. (2021). Engineering Ruthenium-Based Electrocatalysts for Effective Hydrogen Evolution Reaction. *Nano-Micro Letters*,13, 160.

Yu, J., He, Q., Yang, G., Zhou, W., Shao, Z., Ni., Meng. (2019). Recent advances and prospective in ruthenium-based materials for electrochemical water splitting. ACS Catalysis, 9(11), 9973–10011.

Zhang, Z., Jiang, C., Li, P., Yao, K., Zhao, Z., Fan, J., Li, H., Wang, H. (2021). Ruthenium Dichalcogenides: Benchmarking Phases of Ruthenium Dichalcogenides for Electrocatalysis of Hydrogen Evolution: Theoretical and Experimental Insights. *Small*, 17(13), 2170056.

Zheng, Y., Jiao, Y., Zhu, Y., Li, L. H., Han, Y., Chen, Y., Jaroniec, M., Qiao, S.-Z. (2016). High Electrocatalytic Hydrogen Evolution Activity of an Anomalous Ruthenium Catalyst. Journal of the American Chemical Society, 138(49), 16174–16181.

Wei, C., Rao, R. R., Peng, J., Huang, B., Stephens, I. E. L., Risch, M., Xu, Z.J., Shao-Horn, Y. (2019). Recommended Practices and Benchmark Activity for Hydrogen and Oxygen Electrocatalysis in Water Splitting and Fuel Cells. *Advanced Materials*, 1806296.

Wu, H., Huang, Q., Shi, Y., Chang, J., Lu, S. (2023). Electrocatalytic water splitting: Mechanism and electrocatalyst design. *Nano Research*, *16*, 9142–9157.